



Enhancing of Tribological, Mechanical and Microstructural Properties of HVOF Coated AISI 316 Steel by Boriding

AZMI ERDOGAN^{1,5}, ALI GÜNEN², YILDIZ YARALI ÖZBEK,³
and MUSTAFA SABRI GÖK⁴

01.—Department of Metallurgical and Materials Engineering, Faculty of Engineering Architecture and Design, Bartın University, 74100 Bartın, Turkey. 02.—Department of Metallurgy and Materials Engineering, Faculty of Engineering and Natural Sciences, Iskenderun Technical University, 31200 Hatay, Turkey. 03.—Department of Metallurgical and Materials Engineering, Faculty of Engineering, Sakarya University, 54050 Sakarya, Turkey. 04.—Department of Mechanical Engineering, Faculty of Engineering Architecture and Design, Bartın University, 74100 Bartın, Turkey. 5.—e-mail: aerdogan@bartin.edu.tr

Boriding has been attempted to further improve the wear resistance of high-velocity oxygen fuel (HVOF) coatings, often used for corrosion, oxidation or wear resistant applications. For this purpose, different HVOF coatings containing hard phases such as WC and Cr₃C₂ were borided at 900°C for 2 h. The samples were examined in terms of microstructure, nanoindentation mechanical properties and tribological behavior. Boride coatings formed very different boride phases depending on the content of the substrate, and their thickness varies between 8 μm and 20 μm. Although 5–7 times higher hardness values could be obtained with HVOF than the substrate, these values further increased by an average of two times with boriding. The improvement in the wear resistance of AISI 316 with the HVOF is further enhanced by boriding. HVOF coatings showed wear performance according to their hardness. The wear loss ranking of HVOF coatings changed after boriding. In addition to the hardness, which was provided by the boride phases, fracture toughness and residual stresses were also effective in the wear results.

INTRODUCTION

Thermal spray coating methods attract attention in terms of application in oil fields, power plants, drilling operations, mining industries, petrochemical plants and many more because of their many advantages. Depending on the operating conditions, the components used must have superior properties such as corrosion resistance, wear resistance, residual pressure stress, fatigue life and toughness for overloads.¹ HVOF (high-velocity oxygen fuel), one of the thermal spray coating methods, has received great attention in industrial applications such as power plants, oil fields, drilling operations, mining industries, cement production plants, aircraft fields, turbine blades, etc.^{2–4} HVOF-based coatings are currently one of the most widely used surface protection materials for various metallic

components that require a high wear resistance.^{5,6} Depending on the applications and working conditions of the components of industrial equipment, some of these are required to have superior properties, wear and corrosion resistance, fatigue life, residual compressive stress and toughness for extreme loadings.^{5–8} Compared to other thermal spray techniques, the HVOF process can produce powder particles at relatively low temperatures and high speeds, up to three times the speed of sound. So, dense coatings can be formed from the build-up of successive layers of rapidly quenched splats of partially melted or even unmelted particles.⁹

The HVOF process deposits prominently used coatings for wear and friction. Cermet coatings successfully combine the advantages of metals and ceramics and are thus used in the coating industry.^{10,11} The tungsten carbide (WC)-based coatings have been widely used in the field of wear resistance, which could be attributed to the high

(Received May 12, 2023; accepted September 18, 2023;
published online October 10, 2023)

strength, hardness and thermostability of the WC.¹² Especially when coatings containing components such as WC and Cr₃C₂ are deposited by the HVOF process, they can have superior properties such as high toughness, hardness and wear resistance required for certain tribo systems due to their large number of carbide precipitates and fine grained structures.^{3,8,11}

To date, many studies have been conducted on thermochemical processes in which small-sized elements such as C, N and B react and diffuse on the surface to form compounds with superior mechanical behavior. Boriding, one of these processes, has received special attention because of the excellent tribological properties that can be obtained through boride phases.^{13–16} Diffusion of boron to the surface of metals and alloys creates many different types of metallic borides, depending on the process temperature, chemical composition of the substrate materials, used boron source and boriding time. The treatment temperature is also in the range of 973–1273 K, depending on both the input and result parameters.^{17–20} The surface hardness of borided materials can reach very high values depending on the phases formed. However, it should not be forgotten that the boriding process is generally performed on bulk materials.

Different types of HVOF coatings have been tested under many harsh conditions to date. However, although they have superior features, this is not an obstacle for further development. For this purpose, in this study, it was aimed to increase the wear resistance of HVOF coatings by boriding with a strategy that has not been used before. Three different coatings deposited on AISI 316 steel were subjected to boriding process. The produced coatings were investigated in terms of microstructure, nanoindentation and tribological aspects.

EXPERIMENTAL

Commercially purchased (Birçelik Company) AISI 316 austenitic stainless steel with chemical composition of 18–20 wt.% Cr, 10–14 wt.% Ni, 2.0–3.0 wt.% Mo, 2.0 wt.% Mn, 1.0 wt.% Si, 0.08 wt.% C, 0.045 wt.% P, 0.03 wt.% S and balance wt.% Fe was used as the substrate material. Two different powders and their 50–50% mixtures were used for HVOF coating. The first powder used was Woka 7202 and consists of 75% hard phase (Cr₃C₂) and 25% matrix phase (80Ni-20Cr). The other used Diamalloy 2002 powder consists of 50% hard phase (88WC-12Co) and 50% matrix phase (66Ni-18Cr-7Fe-4B-4Si-1C). The HVOF coating process parameters are given in Table I.

After HVOF processing the specimens were cut in a rectangular shape with dimensions 25 mm × 25 mm × 4 mm by utilizing a precision high-speed circular saw. Before boriding process, all surfaces of the specimens were ground with 100 grit SiC emery papers to obtain a smooth surface ($R_a < 0.50 \mu\text{m}$),

Table I. Parameters of HVOF process

Shrouded	400 mm
O ₂	150 slpm
H ₂	300 slpm
Carrier gas	10 (H ₂) slpm
Disc	%15
Velocity (mm/sn)	300 mm/s
Nozzle distance	20 mm
Passes number	5

followed by washing in distilled water, and subsequently sonicated in acetone for 15 min to obtain dirty free surface. The prepared samples were placed in the middle of the crucible made of AISI 321 stainless steel, whose mouth could be closed airtight. Then, the tightly closed crucible was placed in the furnace, which was kept ready at 900°C and held 2 h. At the end of the each boriding heat treatment, the samples were cooled in the furnace from 900°C to 60°C at 5°C per/min, and then the samples were removed from the furnace and left to cool in the open air. Boriding process was carried out by using powder pack method using 90% B₄C + 10% NaBF₄ powder mixture based on our previous studies.^{21,22}

For microstructure investigations, the borided samples were embedded in cold Bakelite. The mounted specimens were subjected to conventional grinding (320–2500 SiC paper) and polishing (6 μm and 3 μm Al₂O₃) processes. The samples were not subjected to any etching process. Thermo Scientific Apreo S scanning electron microscope (SEM) equipped with an EDS (UltraDry) Circular Backscatter (CBS) detector, operating at 30 kV accelerating voltage, was utilized for microstructural views and determining of elemental redistribution on the specimens. The redistribution of alloying elements in boride layers, HVOF layers and matrix was examined by EDS line analysis. The obtained boride layer thicknesses were calculated as means over five measurements taken from the samples' cross-sectional SEM micrographs.

X-ray diffraction (XRD) analysis was conducted to identify the formed of boride phases on the surface. The XRD measurements were performed using a computer-controlled Rigaku SmartLab diffractometer with Cu Ka radiation ($k=1.54 \text{ \AA}$). The 2θ range for scanning was set from 20 to 90, with a step size of 0.02 and a scan speed of 2.0 min⁻¹. The obtained XRD results were analyzed and phase-matched using PDXL software. A Hysitron TI-950 TriboIndenter nanoindenter with a Berkovich tip was used to measure the elastic moduli of the phases and the nanoindentation hardness of the materials. Under a peak load of 10 mN, the tests were conducted in accordance with the Oliver-Pharr analysis method utilizing a 15 analysis matrix.²³ Using a trapezoidal function, force-controlled load-

ing was performed where the load was gradually increased over the course of 30 s, held for 10 s, and then released as stated in the previous studies.²⁴

Wear tests were carried out under dry sliding conditions on TURKYUS POD Ball-on-disc device by following instantaneous friction coefficients. A 6-mm-diameter WC ball was used as an abrasive tip. Five and 15 N loads were determined as wear load. The tests were carried out at a sliding speed of 0.03 m/s, with a total sliding distance of 108 m. The volume losses were calculated by measuring the wear scar widths from at least ten different points. First, the average of the scars formed was calculated. The mean area was calculated depending on the diameter of the ball and the mean scar width. This was multiplied by the scar length to find the volumetric loss. All tests were repeated three times to increase the accuracy of the results. Worn surface images were taken on the TESCAN MAIA3 XMU SEM instrument.

RESULTS AND DISCUSSION

XRD and SEM-EDS Analyses

In Fig. 1, XRD analyses of samples of AISI 316 steel and HVOF coatings subjected to boriding treatment at 900°C for 2 h are given. After the boriding process applied to AISI 316 steel (Fig. 1a), it was determined that the dominant phase on the surface was FeB, as well as Fe₂B, CrB and Ni₃B phases. Considering the boriding studies on AISI 316 steel in the literature, many studies have reported that FeB and Fe₂B^{13,19,25–27} phases were detected. However, CrB,^{13,19,26} Cr₂B,^{13,19,26} NiB,¹⁹ Cr₅B₃²⁷ phases are also frequently formed depending on boriding conditions.

In the boriding process of HVOF coatings at 900°C for 2 h, many different phases were determined depending on the component differences. After the boriding process of Diamalloy 2002 HVOF coating (Fig. 1b), NiB, CrB, Cr₂Ni₃B₆, CoWB, Cr₅B₃, W₂B, Co₂B and Co₃B boride phases were detected on the surface, as well as WC and Cr_{0.8}Ni_{0.2} phases originating from HVOF coatings. As a result of the boriding process applied to the coating formed with HVOF in 50% Diamalloy+50% Woka powders (Fig. 1c), Cr₇C₃ peak from the HVOF coating was detected besides CrB, NiB, Cr₂Ni₃B₆, Co₃B, Co₂B and CoWB borides. The fact that WC was not detected in the XRD analysis despite the presence of WC in the powder content is thought to be because the WC diffuses towards the inner parts from the near-surface areas, as seen in the SEM-EDS line analyses. After boriding the Woka 7202 HVOF coated sample, NiB, CrB, Cr₂Ni₃B₆ and Cr₅B₃ borides are present (Fig. 1d). In addition, peaks belonging to the Cr₇C₃ and Cr₂C₃ phases formed in the HVOF coating were also encountered. Moreover, Cr₂O₃ and Cr₃O oxide peaks were detected because of the open-air boriding process.

Considering Fig. 2, it was determined that the boride layer formed in three main regions at different concentrations in accordance with the studies carried out on the boriding of stainless steels.^{13,26,28–31} These regions can be listed as FeB layer (darker), Fe₂B (lighter) and diffusion layer (where there are boride formations in places) from the surface to the interior, respectively, as shown in Fig. 2. As can be easily seen from the SEM-EDS line analysis, the thicknesses of FeB and Fe₂B and diffusion zone layers are around 15 μm, 5 μm and 11 μm, respectively. In borided steels, a single-phase Fe₂B layer is more desirable than FeB+Fe₂B formation because, when the temperature of the samples is lowered to room temperature after boriding at high temperatures, the Fe₂B phase is exposed to high compressive stress and the FeB phase is exposed to high tensile stress. This may cause crack formation at the interface of FeB-Fe₂B phases with different thermal expansion coefficients. Such crack formation can cause interlayer degradation and, furthermore, biphasic layer separation. Homogenization process can be applied to reduce crack formation or boriding process can be applied by selecting suitable temperature, time and powder mixtures to control Fe₂B and FeB phase formation.^{32–34} The fact that the boride layer obtained in the study is continuous along the surface and does not contain any cracks or separations between FeB and Fe₂B shows that the boriding parameters applied are correctly selected. The EDS line analysis shows that the Fe, Cr and Ni elements in AISI 316 follow a different course in the boride layer because of the boriding process. Namely, although the boride layer is mostly composed of Fe and B, there is also the presence of Cr and Ni in it. However, this ratio is lower than the 316 steel content. This is consistent with the phase structure detected in the XRD analyses presented in Fig. 1a.

A 11.77±1.8-μm-thick boride layer, consisting of a high proportion of Cr, Ni and B, is formed on the surface with the boriding process applied on the surface on which Diamalloy 2002 powder is deposited by the HVOF method (Fig. 3). Under the boride layer, there is a 122.55±4.3-μm-thick HVOF coating layer with a chemical composition compatible with the Diamalloy 2002 powder content. Diamalloy 2002 HVOF coating exhibited a layer with good structural homogeneity. In addition, the coating and its interface with the substrate exhibited very few cracks and voids compared to the Woka 7202 coating. An AISI 316 matrix under this layer is clearly seen.

The SEM view and EDS line analysis of the borided sample after HVOF coating, which was deposited using 50% Diamalloy 2002+50% Woka 7202 powder, are given in Fig. 4. A thin boride layer with a thickness of 8.74 μm±2.2 μm, consisting mainly of Cr and B, was detected on the surface. Notably, among the coating powder contents (W, Ni, Cr, Co) used in HVOF coating, only Cr is included in the

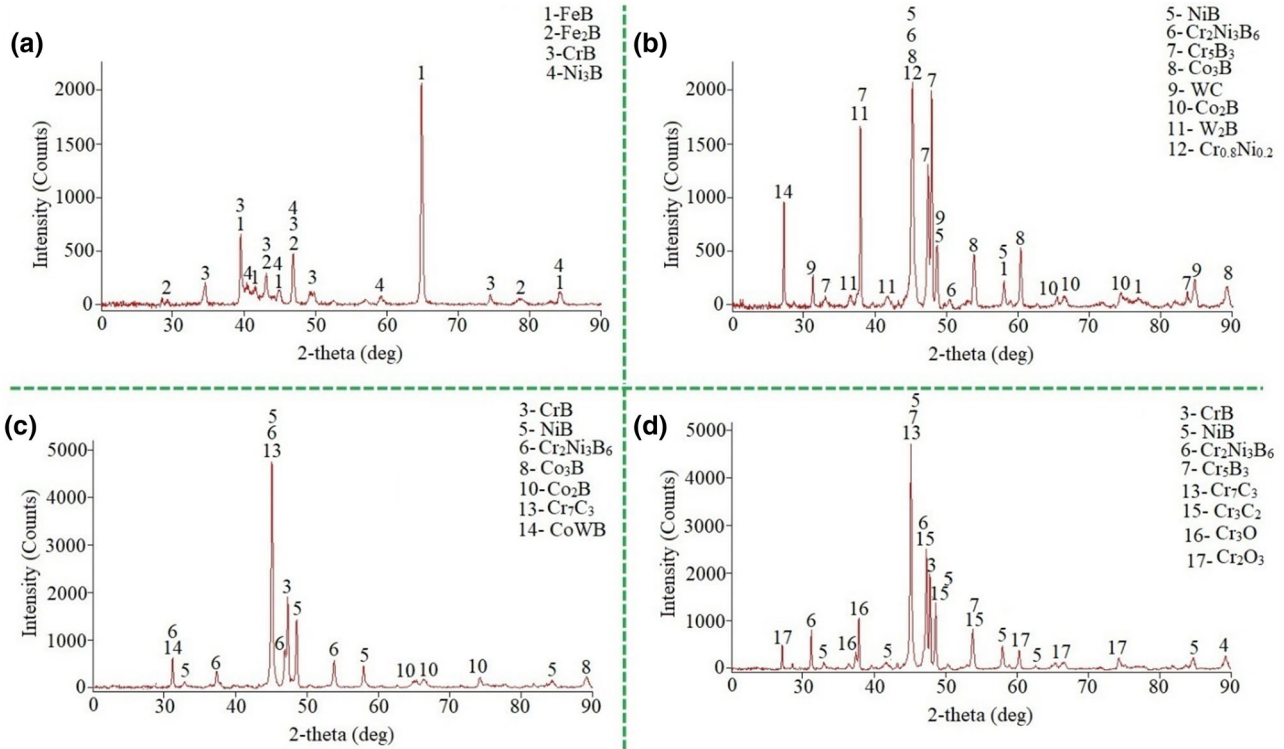


Fig. 1. XRD patterns of samples after boriding at 900°C for 2 h: (a) AISI 316, (b) Diamalloy 2002, (c) 50% Diamalloy 2002+50% Woka 7202, (d) Woka 7202 HVOF.

boride layer content. This situation is related to the diffusion of Cr atom with low atomic weight towards the surface, while elements with higher atomic weight such as W, Ni and Co diffuse towards the interior parts in boriding process.³⁵ Under the boride layer, it was observed that a coating layer with a chemical composition compatible with the powders used in HVOF (50% Diamalloy 2002+50% Woka 7202) with a thickness of $175.96 \mu\text{m} \pm 8.9 \mu\text{m}$ was obtained. The coating morphology made from mixed powders looks slightly different from the pure powder structure. More porosity and voids are formed in the mixture of the two powders. This is normal; the grain size differences in the mixed powders may result in slightly larger voids. The structure of HVOF coatings obtained with pure powders is denser. However, it is possible to talk about the formation of voids caused by melting in some regions. The pictures show that the sand-blasting process applied to the stainless steel surface is successful and that the coating and substrate are well bonded.

When the SEM view and EDS line analysis of the borided sample after HVOF coating, deposited using Woka 7202 powder, were examined (Fig. 5), a thin boride layer, $10.93 \mu\text{m} \pm 1.9 \mu\text{m}$ thick, mostly composed of Cr, Ni and B, was detected on the surface. The O₂ ratio is low in the boride layer content. This is because the alloying elements in the powder used

in the HVOF coating consist only of Ni, Cr and C. Below the boride layer, a coating layer with a chemical composition compatible with the powders used in HVOF (Woka 7202) with $144.36 \mu\text{m} \pm 7.1 \mu\text{m}$ thickness is observed. At the bottom of the coatings, there is an AISI 316 substrate.

Nanoindentation Properties

Hardness-elasticity values, which are an important criterion in determining the mechanical properties of coatings (Table II), were determined by nanoindentation technique. Table I indicates that the hardness values in the borided layer of the borided AISI 316 steel are in the range of 23.89–24.91 GPa and are compatible with the hardness values obtained on the borided stainless steels in the literature.³⁶ The hardness value of the obtained boride layer is higher than the hardness values obtained with the FeB and Fe₂B phases. This can be explained by the XRD and EDS line analyses given in Figs. 1, 2. Due to the presence of Cr in the boride layer and therefore the Cr₅B₃ phase, whose formation in the structure was determined by XRD analysis, the hardness values increased even more. The hardness values of the boride layers obtained on the HVOF coatings indicated that the hardness values vary according to the contents of the coatings. Because the content of Woka 7202 powder is mostly composed of Ni and Cr, the hardness values of the



Fig. 2. Section analysis of the boride layer obtained on the surface of AISI 316 steel because of boriding at 900°C for 2 h: SEM view and EDS line analysis.

boride layer formed on the surface of this sample are slightly lower, with an average of 17.64 GPa. The hardness value of the layer in the region where this coating layer consists of phases such as Cr₇C₃, Cr₃C₂ is in the range of 7.50–13.62 GPa. The hardness of the boride layer formed on Diamalloy 2002 HVOF is in the range of 20.53–21.92 GPa. Higher hardness values can be attributed to the

formation of hard phases such as W₂B, Cr₅B₃ and Co₃B as indicated in XRD analysis of W, Co and Cr elements in Diamalloy powder content. Studies in the literature reported that the precipitation of Cr-B-containing phases between carbide grains provides increasing solute concentrations in these regions.³⁷ Thus, finely precipitated CrB prevents the dislocation movement of Cr₅B₃ phases and provides

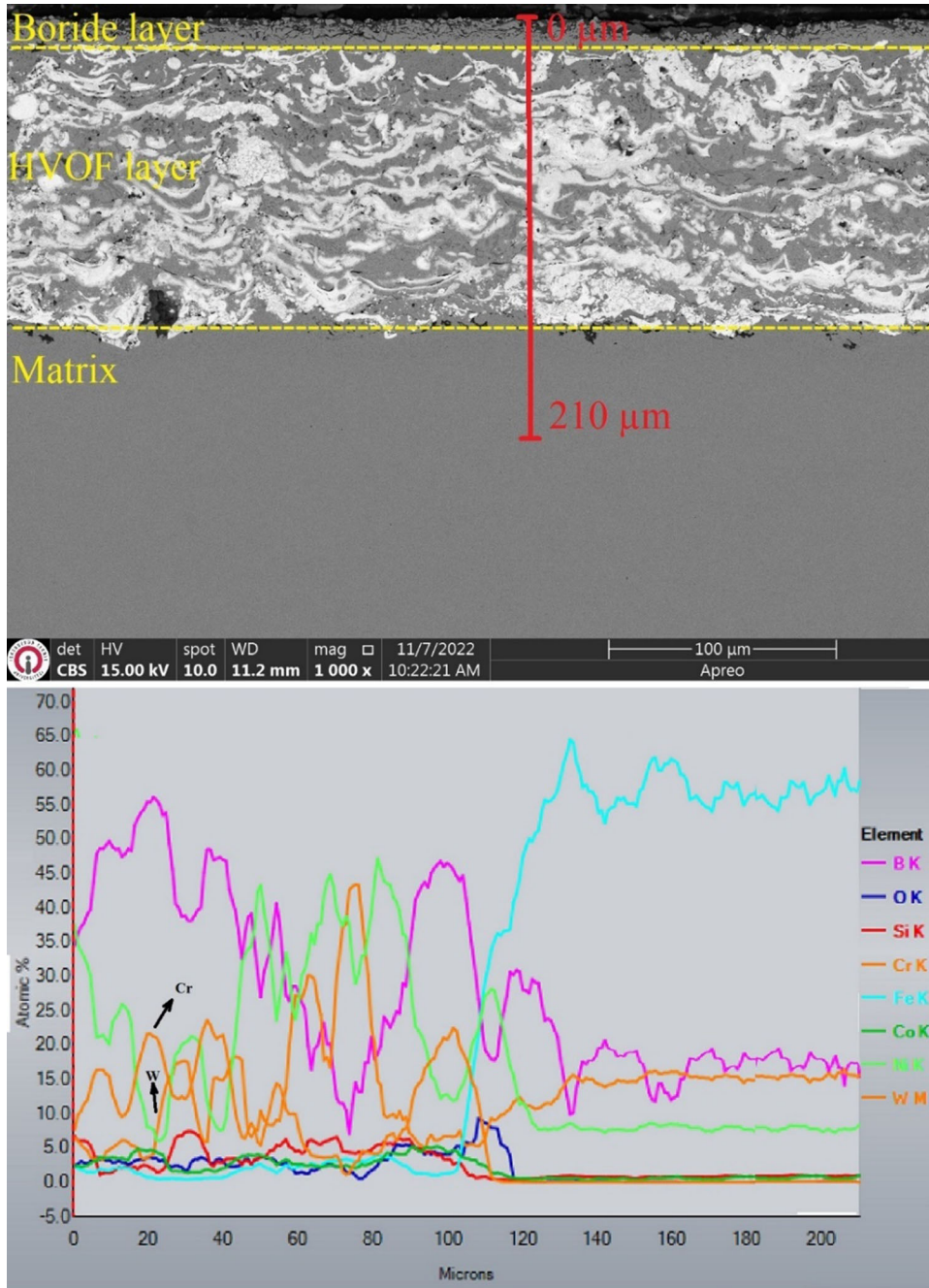


Fig. 3. Section analysis of the boride layer obtained on the Diamalloy 2002 HVOF coating as a result of boriding at 900°C for 2 h: SEM view and EDS line analysis.

an improvement in the hardness values of the coatings.^{38,39} The hardness values in the boride layer of the coatings obtained with the 50% mixture of Diamalloy 2002 and Woka 7202 powders were 29.40–33.21 GPa, and it was the sample with the highest hardness value. This situation is attributed to the presence of many components that can form a phase with boron due to the use of both powders. The distortion effect created by a wide variety of

boride phases is thought to be the most important cause of high hardness.

Apart from the hardness, one of the most important values that can be obtained from Table II is the residual stresses that can be understood depending on the h_f/h_{max} ratio. The h_f/h_{max} ratios are comparatively lower in the boride columns compared to the HVOF coating layer and AISI 316 matrix, as shown in Table II. This indicates that the boride

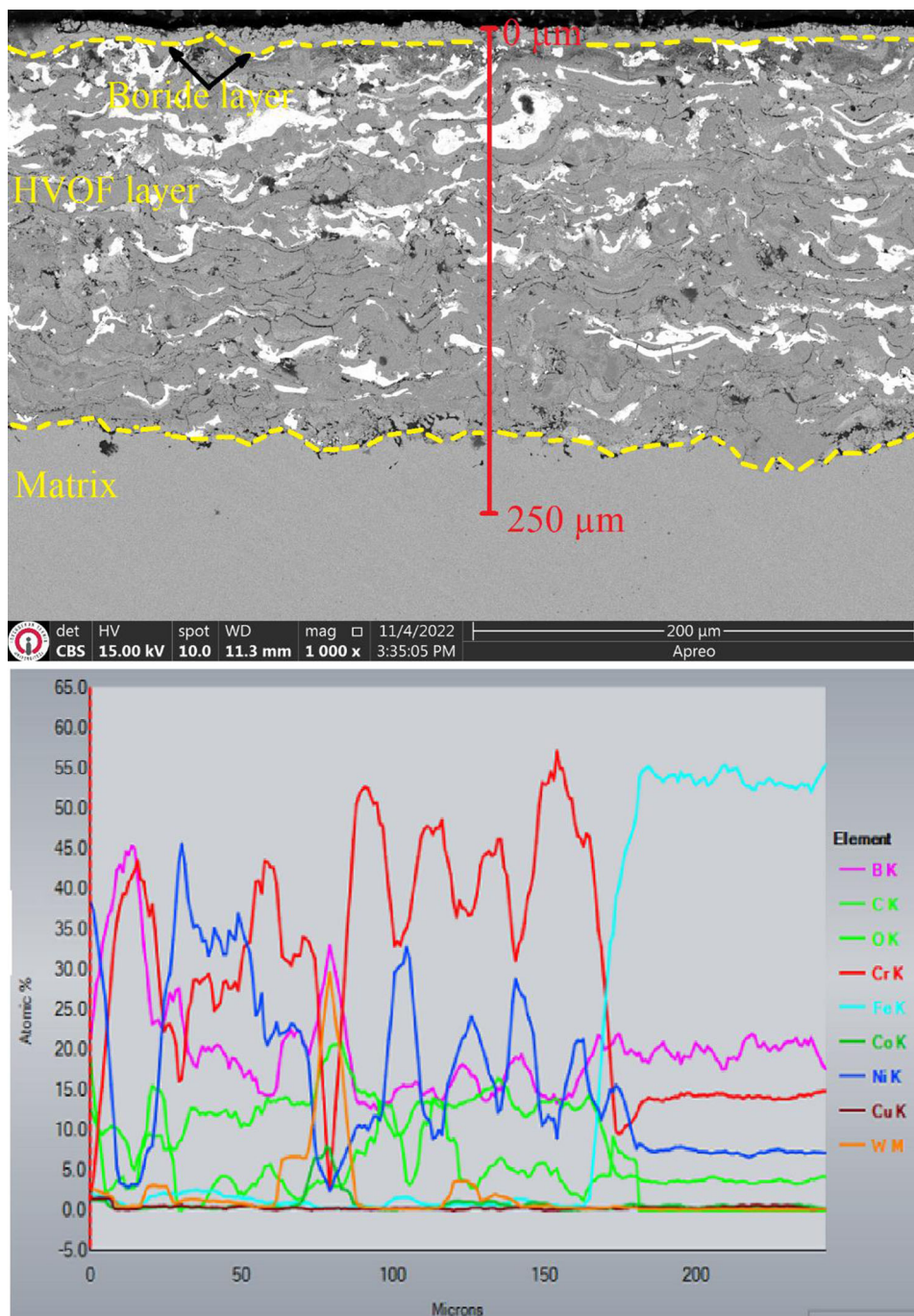


Fig. 4. Section analysis of the boride layer obtained on the 50% Diamalloy 2002+50%Woka 7202 HVOF coating because of boriding at 900°C for 2 h: SEM view and EDS line analysis.

regions exhibit higher elastic recovery and residual stress.⁴⁰ This behavior is attributed to the fragile nature of boride contributions to these characteristics. The differences in hf/h_{max} ratios because of boriding thermal spray coatings formed with HVOF powders can be attributed to the different phase structures formed as a result of boriding. The results obtained in Table II support this point. Con-

sidering the hf/h_{max} values, the borided sample from the mixed powders shows the lowest value (0.34–0.35). A low hf/h_{max} ratio indicates higher residual stresses in the coating layers.^{36,40} Notably, the hf/h_{max} ratios of the boride layers formed on Diamalloy (0.44) and Woka (0.48) powders are higher than those on borided AISI 316 steel (0.39), suggesting lower residual stresses in the former.

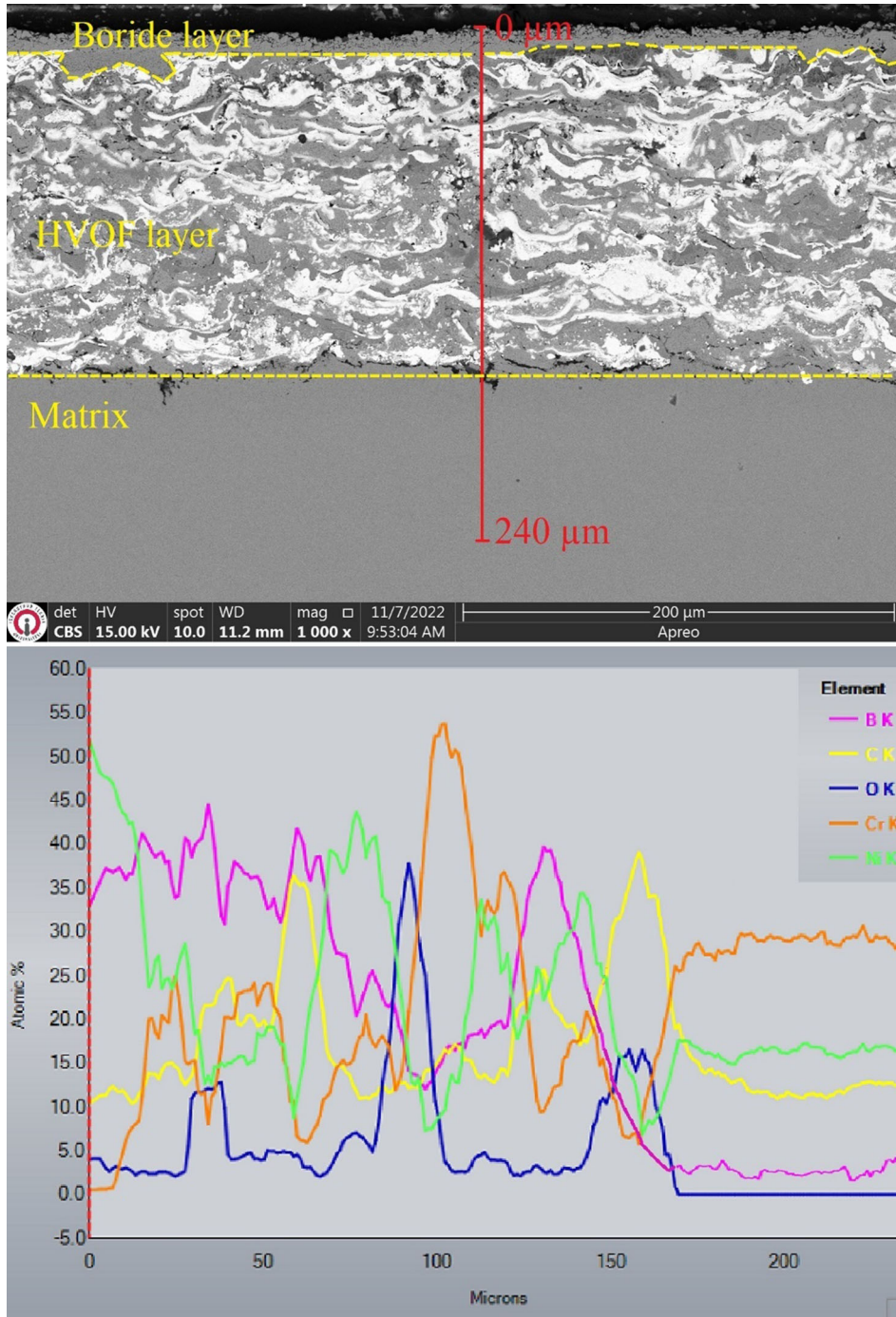


Fig. 5. Section analysis of the boride layer obtained on the Woka 7202 HVOF coating because of boriding at 900°C for 2 h: SEM view and EDS line analysis.

Another parameter for assessing material performance using nanoindentation measurements is the H/E^2 ratio, which reflects a material's resistance to plastic deformation by measuring contact hardness (dP/dh).^{41,42} Table II shows that the H/E^2 ratio is enhanced with HVOF coatings compared to the untreated material. Furthermore, the H/E^2 value is further improved with the subsequent boriding heat

treatment applied after HVOF, resulting in increased surface performance against plastic deformation through both HVOF and boriding processes.

Dry Sliding Wear Properties

The volume losses occurring because of the abrasion tests of AISI 316 stainless steel, HVOF coatings

Table II. Nanoindentation data obtained in the experiments on the boride layer, HVOF layer and matrix

Borided AISI 316	h_c (nm)	P_{max} (μN)	h_{max} (nm)	h_f (nm)	E_r (GPa)	H (GPa)	h_f/h_{max}	H/E^2
Boride layer1	109.51	10067.16	165.57	64.19	189.71	24.91	0.39	0.00069
Boride layer2	112.11	10066.45	167.39	65.91	189.50	23.89	0.39	0.00066
Matrix1	235.18	10079.30	285.12	201.88	106.17	6.21	0.71	0.00055
Matrix2	235.89	10078.00	283.35	201.90	111.69	6.17	0.71	0.00049
Diamalloy 2002	h_c (nm)	P_{max} (μN)	h_{max} (nm)	h_f (nm)	E_r (GPa)	H (GPa)	h_f/h_{max}	H/E^2
Boride layer1	122.04	10068.11	177.40	78.03	175.34	20.53	0.44	0.00066
Boride layer2	117.64	10066.52	171.13	75.02	187.15	21.92	0.44	0.00063
HVOF layer1	194.12	10077.23	252.93	152.58	107.99	8.85	0.60	0.00075
HVOF layer2	131.91	10070.65	188.10	87.71	159.84	17.86	0.47	0.00069
HVOF layer3	114.23	10068.42	163.23	76.48	209.34	23.11	0.47	0.00052
Matrix1	238.75	10075.18	282.74	208.22	119.07	6.03	0.74	0.00042
Matrix2	276.03	10076.86	318.23	244.23	108.58	4.60	0.77	0.00039
50% Diamalloy 2002 + 50% Woka 7202	h_c (nm)	P_{max} (μN)	h_{max} (nm)	h_f (nm)	E_r (GPa)	H (GPa)	h_f/h_{max}	H/E^2
Boride layer1	93.05	10,067.51	154.65	52.18	197.06	33.21	0.34	0.00085
Boride layer2	99.73	10,067.25	161.54	56.39	186.83	29.40	0.35	0.00084
HVOF layer1	107.79	10,066.74	166.95	64.75	181.77	25.62	0.39	0.00077
HVOF layer2	125.38	10,066.78	179.27	72.64	174.93	19.56	0.41	0.00063
HVOF layer3	119.79	10,067.18	184.79	73.31	150.85	21.23	0.40	0.00093
Matrix1	246.43	10,077.84	297.93	206.87	99.96	5.69	0.69	0.00056
Matrix2	250.36	10,077.29	301.50	212.20	98.76	5.52	0.70	0.00056
Woka 7002	h_c (nm)	P_{max} (μN)	h_{max} (nm)	h_f (nm)	E_r (GPa)	H (GPa)	h_f/h_{max}	H/E^2
Boride layer1	132.84	10,070.93	190.22	90.61	156.54	17.64	0.48	0.00071
Boride layer2	132.84	10,070.93	190.22	90.61	156.54	17.64	0.48	0.00071
HVOF layer1	212.35	10,076.62	258.84	180.55	126.53	7.50	0.70	0.00046
HVOF layer2	201.47	10,074.85	249.38	164.00	128.59	8.26	0.66	0.00049
HVOF layer3	153.27	10,071.11	206.11	120.17	149.77	13.62	0.58	0.00060
Matrix1	266.40	10,081.03	311.66	234.09	104.59	4.92	0.75	0.00044
Matrix2	266.01	10,079.70	309.02	234.63	110.44	4.93	0.76	0.00040

hc: contact depth, hmax: maximum depth, Er: reduced elastic modulus, H: nano-hardness, hf: final displacement, P_{max}: applied load.

and borided samples are given in Fig. 6a. The main purpose of this study is to determine how the wear properties of different types of HVOF coatings change with the boriding process. In addition, AISI 316 steel was also borided for use as a reference. Thus, it was possible to compare the results obtained from the coatings produced by the HVOF method with the borided AISI 316 steel. Examining the volume losses in Fig. 6 shows that the AISI 316 steel used as the substrate gives the highest wear losses as expected. It is normal for this backing material with an average hardness of 200 HV to show the highest volume loss. As a result of the wear tests, HVOF coatings showed less wear loss than the substrate material. The hardnesses of HVOF coatings are on average 1500 HV, 1020 HV and 1200 HV for Diamalloy 2002, Woka 7202 and 50% mix, respectively. There is an average increase of 5-8 times compared to the litter. Naturally, it is possible to attribute the decrease in wear losses to

this. When HVOF coatings were evaluated by themselves, results proportional to hardness were obtained. Diamalloy 2002 with the highest hardness gave the lowest volume loss, while Woka 7202 with the lowest hardness gave the highest wear losses. These results have been frequently encountered in the literature before. Although HVOF coatings generally have a porous structure, they show better wear resistance due to their high hardness. For example, Zhang et al.⁴³ demonstrated that the HVOF sprayed Fe48Mo14Cr15Y2C15B6 coating showed better wear resistance than AISI 1040 steel, and Koga et al.⁴⁴ demonstrated that the Fe60Cr8Nb8B24 HVOF coating showed better wear resistance than AISI 430 stainless steel. Moreover, similar HVOF coatings used in this study can be given as examples. For example, it was determined by Wang et al.⁴⁵ and Ma et al.⁴⁶ that the HVOF sprayed WC-12Co coating showed better wear resistance than mild steel and bearing steel. In some

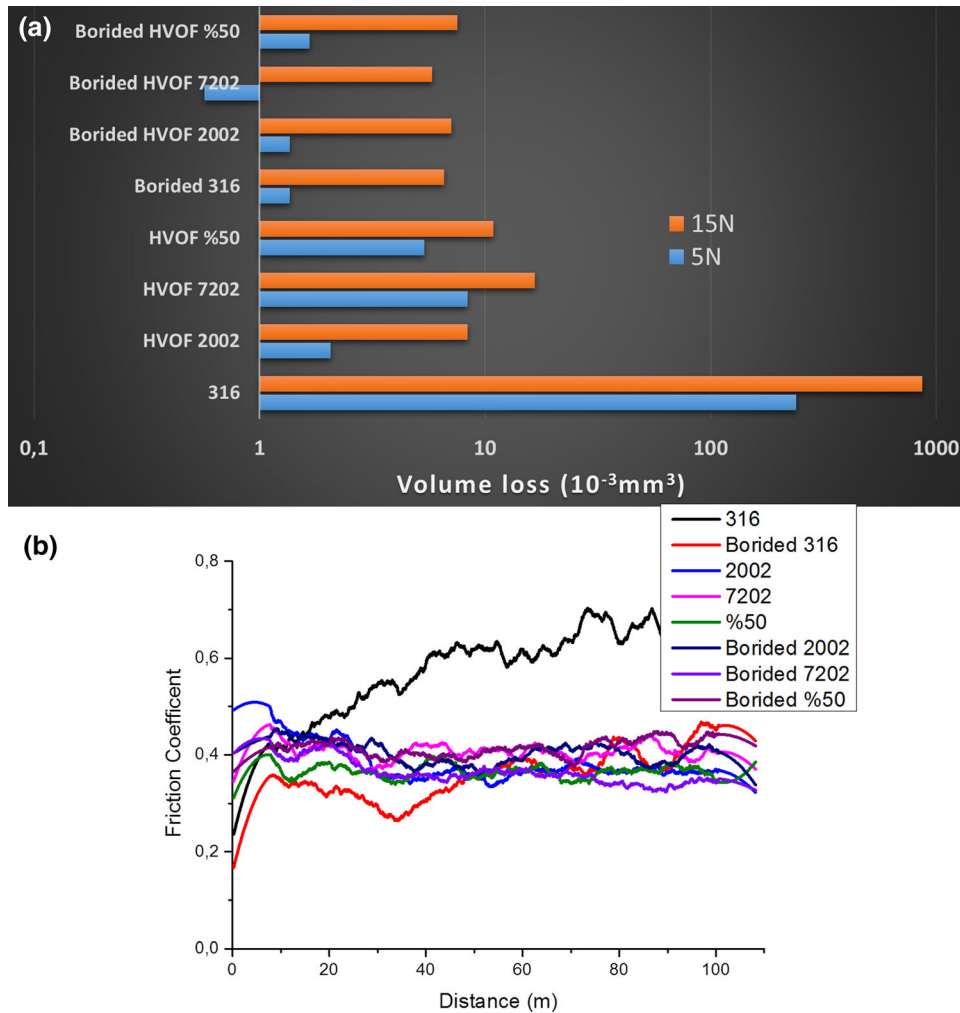


Fig. 6. (a) Volume losses and (b) friction coefficient curves in ball-on disc wear tests under 15 N.

studies, the wear resistance of the powders used in this study was investigated comparatively.^{47–49}

The difference of this study from the studies mentioned above is determining the change in wear resistance of borided HVOF coatings. In general, if we need to compare the wear resistance, the boriding process has provided an improvement in the wear resistance of all samples. In the studies conducted in the literature, only one study examined the effect of boriding process on HVOF coating. Lindner et al.⁶ deposited Inconel 625 alloy on AISI 316L steel in a study and conducted boriding treatment on this coating. In their wear tests, they determined that boriding process reduces wear losses. In this study, the performance of HVOF coatings with a much harder structure was tested. We also tested 316 steel, which is only borided, giving a clearer approach to the performance of borided HVOF coatings. Looking at the results, the volume losses in all samples decreased with the increase in hardness provided by the boriding process. While the boriding process of AISI 316 steel provides a reduction of up to 99% in volume loss, a 16–94%

reduction in volume losses has been achieved in different types of HVOF coatings with the boriding process. Considering these results, the boriding process increases the wear resistance under all conditions. The natural reason for this is the hard and wear-resistant structures formed by different boride phases formed by boriding. From this point of view, it has been shown that it is possible to increase the wear resistance of even very hard HVOF coatings by boriding. When the borided samples are examined, different results are obtained compared to before boriding. Before boriding, a wear resistance parallel to hardness was observed, but this situation changed after boriding process. While the best wear resistance was seen in borided HVOF 7202 sample, the lowest wear resistance was seen in borided HVOF 50% sample. The borided 50% HVOF coating has the highest hardness, while the borided HVOF Woka 7202 sample has the lowest. In this case, it is possible to say that hardness is not the most important factor in wear resistance after boriding. The wear resistance increase after boriding compared to before boriding is directly related to

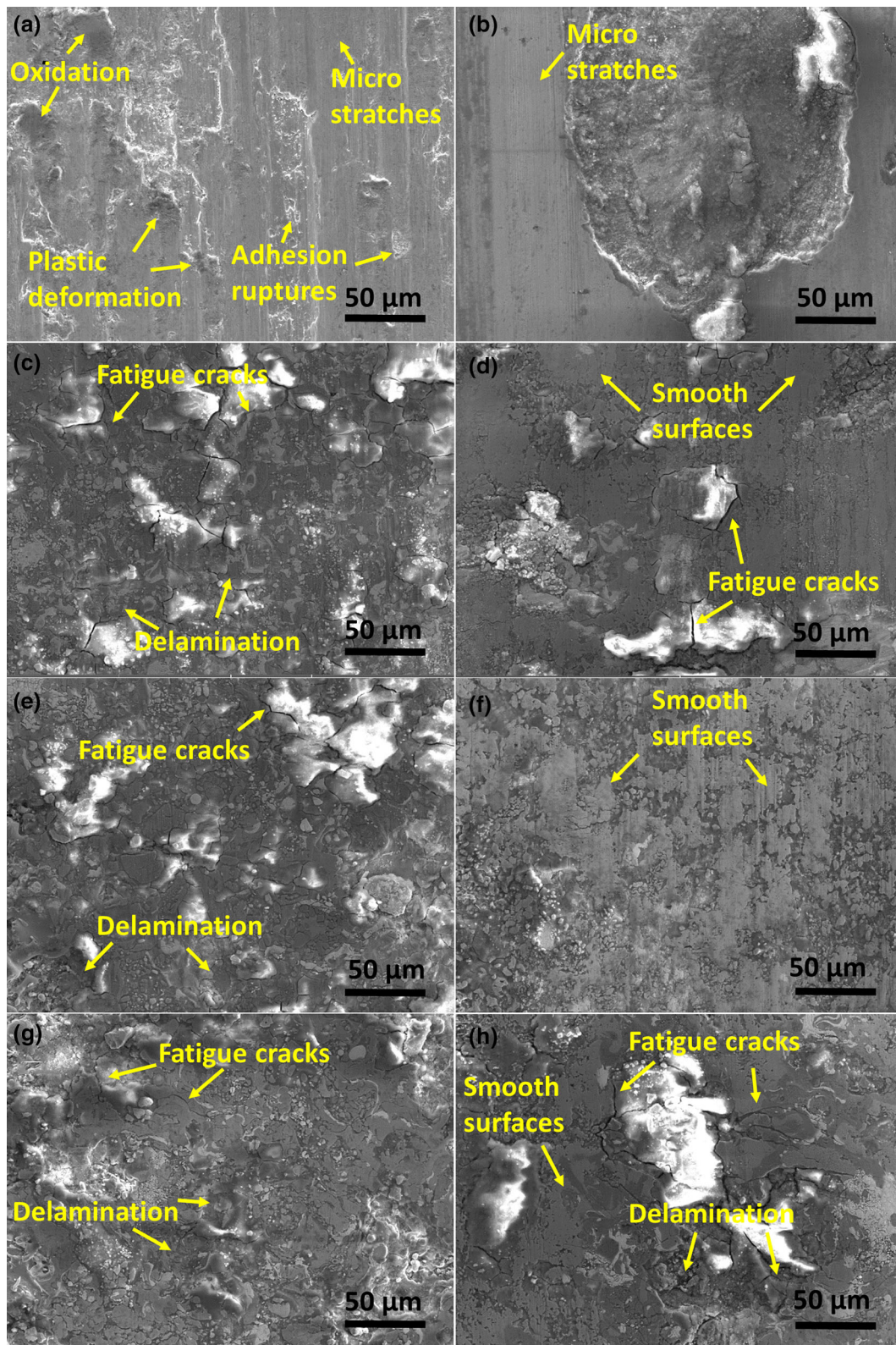


Fig. 7. SEM images of the worn surface of the samples: (a) AISI 316, (b) borided AISI 316, (c) HVOF Diamalloy 2002, (d) borided HVOF Diamalloy 2002, (e) HVOF Woka 7202, (f) borided HVOF Woka 7202, (g) 50% HVOF, (h) borided 50% HVOF.

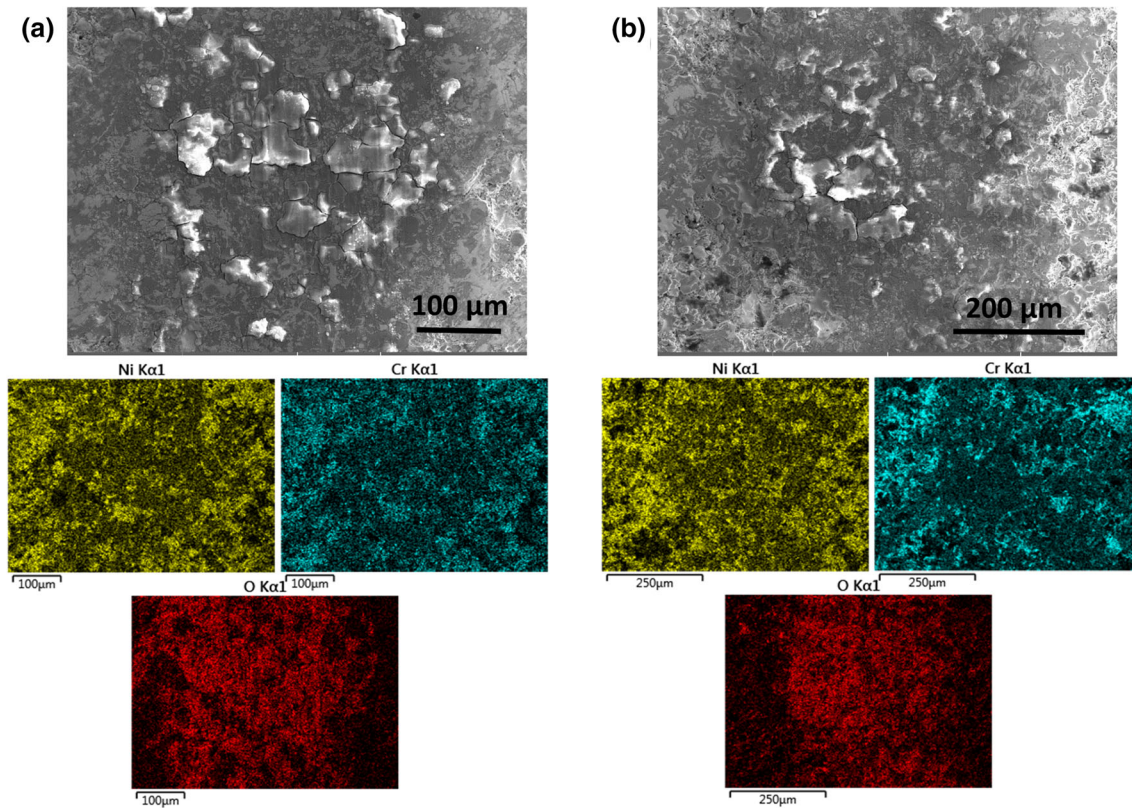


Fig. 8. Wear trace EDS map analysis for (a) HVOF Diamalloy 2002 and (b) HVOF Woka 7202.

the increase in hardness. However, the difference in wear resistance of borided samples should be explained by other factors. First, fracture toughness should be mentioned here. It is possible that the very high hardness seen in the borided HVOF 50% sample also causes a low fracture toughness. After boriding, a decrease in fracture toughness occurs and the problems caused by this in wear resistance are known.^{14,15,50} It is possible that the same problem has been encountered here as well. Very high hardness values may have caused low fracture toughness, which affects wear resistance especially at high loads. Another factor is the residual stresses that occur in the coatings. It has been previously stated that a high h_f/h_{max} ratio means low residual stresses. The h_f/h_{max} ratios in Table II show why different results occur in wear losses than expected according to hardness. The high residual stresses were effective in the wear resistance examined under cyclic loads and caused an increase in the wear losses of the samples with high residual stresses.

The friction coefficient curves are given in Fig. 6b. When examined, the friction coefficients occurred close to each other and averaged between 0.3 and 0.4 in all samples except AISI 316. The graph shows that AISI 316 steel is clearly decomposed and generally increasing. Of course, this increase and high values in the curve can be associated with the weak wear resistance of AISI 316 steel. Due to a large wear track and continuously increasing track width,

ball movement became increasingly difficult, resulting in a continuous increase in the friction coefficient. The coefficient of friction of HVOF coatings and borided HVOF coatings generally increased at the beginning of the test and then decreased slightly to average values. The increase at the beginning of the test can be explained by the contact area and contact pressure. Many earlier studies explained that the friction coefficient increases with the increase of the test area, which is low at the beginning of the test and then becomes stationary.^{51,52} The subsequent decrease can be attributed to oxidation due to the instantaneous temperature rise under cyclic loading.⁵³ Oxidation, which occurs because of the instantaneous temperature increase, helps to reduce the friction coefficient by forming a lubricating layer.^{54,55}

SEM images of the wear trace, which occurred because of the wear tests, are given in Fig. 7. More than one wear mechanism can be mentioned on the untreated AISI 316 surface (Fig. 7a). With a small amount of plastic deformation and oxidation, adhesion ruptures are seen in some areas. In addition, there are micro scratches caused by wear debris due to the low hardness of the material. After the boriding process, a very different worn surface mechanisms appearance (Fig. 7b) occurred. Although most of the worn surface is smooth and contains a very small amount of micro-scratches, there are spills in some areas, as can be seen from

the figure. It has been mentioned before that the brittleness of surfaces increases because of increased hardness. The spills seen here can be attributed to this. The borided surface has a high brittleness, and the plastic deformation ability is low. However, repeated loads during wear can also create cracks under the surface. As these cracks come to the surface and coalesce over time, spill areas may occur as seen on the surface. The formation of these spills is also reflected in the coefficient of friction. The friction coefficient values, which were low towards the middle of the test, started to increase over time. This rise can be associated with the spills seen on the surface.

When we look at the worn surfaces of HVOF coatings (Fig. 7c, e and g), similar wear mechanisms can be mentioned. A high rate of oxidation is observed on the surface of all HVOF coatings. The high rate of oxidation occurring on the worn surfaces of HVOF Diamalloy 2002 and HVOF Woka 7202 samples can be seen in Fig. 8. Material loss due to delamination has occurred. The brittleness of the already high hardness HVOF coatings is further increased by the occurrence of oxidation. Fatigue cracks have occurred because the surface is constantly exposed to cyclic loads during wear. These cracks coalesce more rapidly because of the relatively low plastic deformation ability of the coating and the oxide layer. With this merger, the delamination wear mechanism has emerged. Although there are generally similar wear mechanisms after boriding, there are changes in parallel with wear losses. For example, the borided Diamalloy 2002 surface (Fig. 7d) and the borided 50% sample surface (Fig. 7h) have smooth surfaces with fatigue cracks and delamination. These smooth surfaces are also an indication of increased wear resistance. However, due to the damage mechanisms that still exist on the surface, a reverse situation has emerged compared to before boriding. Woka 7202 sample, which showed the lowest wear resistance among HVOF coatings before boriding, showed the best wear resistance after boriding. This shows that on the surface of the borided Woka 7202 sample (Fig. 7f), these smooth surfaces covered more area. This also explains why this sample shows the lowest wear loss. One of the reasons why cracks and delamination are not visible on the surface is the low residual stresses in this sample.

CONCLUSION

We have brought a new approach to HVOF coatings with this study to determine how tribological properties change with boriding of HVOF coatings. In addition, a clear approach has been shown to the wear performance by making a comparison with AISI 316 steel, which is only subjected to boriding process. More realistic results have been obtained regarding the effect of boriding process, especially by using HVOF coatings with high hardness. Con-

sidering the wear performances, it has been proven that boriding process can be used in HVOF coatings that will try to wear. The results obtained are briefly summarized below.

- In XRD examinations, Fe-Fe₂B phases were detected on AISI 316 steel after boriding. In HVOF coatings, boride phases containing Fe, Ni, Cr, Co and W were formed in accordance with the chemical content.
- In SEM analysis, an approximately 20- μ m-thick boride layer was determined in AISI 316 steel, while approximately 11- μ m, 9- μ m and 11- μ m-thick boride layers were determined in Diamalloy, 50% and Woka HVOF coatings, respectively.
- After the boriding process, hardness values of up to 25 GPa, 22 GPa, 33 GPa and 18 GPa were obtained on AISI 316 steel, HVOF-Diamalloy, HVOF-50% and HVOF-7202 coatings, respectively. In terms of residual stresses in the boride layer, the sequence was occurred as “50% > AISI 316 > Diamalloy > Woka.”
- While HVOF coatings show better wear resistance than AISI 316, wear resistance is further improved by boriding. Although hardness is the most important factor, fracture toughness and residual stresses are other important factors affecting wear losses.

CONFLICT OF INTEREST

On behalf of all authors, the corresponding author states that there is no conflict of interest.

REFERENCES

1. M. Jalali Aizpour and M. Tolouei-Rad, *Ceram. Int.* 45, 13934 (2019).
2. S.M.M.M. Shabana, M.M.M. Sarcar, K.N.S. Suman, and S. Kamaluddin, *Mater. Today Proc.* 2, 2654 (2015).
3. H. Wang, Q. Qiu, M. Gee, C. Hou, X. Liu, and X. Song, *Mater. Des.* 191, 108586 (2020).
4. R. Khuengpukheiw, A. Wisitorsaat, and C. Saikaew, *Wear* 484–485, 203699 (2021).
5. B.J.M. Freitas, V.A. de Oliveira, P. Gargarella, G.Y. Koga, and C. Bolfarini, *Surf. Coat. Technol.* 426, 127779 (2021).
6. T. Lindner, M. Löbel, R. Hunger, R. Berger, and T. Lampke, *Surf. Coat. Technol.* 404, 126456 (2020).
7. P. Jayashree, S. Turani, and G. Straffelini, *Wear* 464–465, 203553 (2021).
8. Q. Wang, S. Luo, S. Wang, H. Wang, and C.S. Ramachandran, *Int. J. Refract. Met. Hard Mater.* 81, 242 (2019).
9. S. Hong, J. Qin, J. Lin, Y. Wu, J. Li, and Y. Zheng, *J. Mater. Res. Technol.* 21, 1507 (2022).
10. F. Pougoum, L. Martinu, P. Desjardins, J. Klemberg-Sapieha, S. Gaudet, S. Savoie, and R. Schulz, *Wear* 358–359, 97 (2016).
11. F. Pougoum, L. Martinu, J.E. Klemberg-Sapieha, S. Savoie, and R. Schulz, *Surf. Coat. Technol.* 307, 109 (2016).
12. Y. Wang, W. Zhang, D. Chen, X. Liu, W. Hu, L. Liu, J. Yan, and X. Xiong, *Surf. Coat. Technol.* 407, 126766 (2021).
13. L.A. Arteaga-Hernandez, C.A. Cuao-Moreu, C.E. Gonzalez-Rivera, M. Alvarez-Vera, J.A. Ortega-Saenz, and M.A.L. Hernandez-Rodriguez, *Wear* 477, 203825 (2021).
14. A. Erdogan, B. Kursuncu, A. Günen, M. Kalkandelen, and M.S. Gök, *Surf. Coat. Technol.* 386, 125482 (2020).
15. A. Erdoğan, *Surf. Coat. Technol.* 357, 886 (2019).

16. A. Gunen, M. Keddama, S.E. Sunbul, K. Icin, K.M. Doleker, M.S. Gok, S. Dal, and A. Erdogan, *J. Alloys Compd.* 929, 167310 (2022).
17. A. Günen, M. Keddama, A. Erdoğan, and M. S. Karakaş, *Met. Mater. Int.* 1 (2021).
18. A. Erdogan, *J. Tribol.* 141, (2019).
19. Y. Kayalı and Y. Yalçın, *I*, 12 (2020).
20. H. Cimenoglu, E. Atar, and A. Motallebzadeh, *Wear* 309, 152 (2014).
21. A. Günen, K.M. Döleker, M.E. Korkmaz, M.S. Gök, and A. Erdogan, *Surf. Coat. Technol.* 409, 126906 (2021).
22. Y. Kanca, M.C. Uçgun, and A. Günen, *Metall. Mater. Trans. A Phys. Metall. Mater. Sci.* 54, 671 (2022).
23. W.C. Oliver and G.M. Pharr, *MRS Bull.* 35, 897 (2010).
24. A. Günen, F. Ceritbinmez, K. Patel, M.A. Akhtar, S. Mukherjee, E. Kanca, and M.S. Karakas, *CIRP Manuf. Sci. Technol.* 38, 547 (2022).
25. M. Keddama and P. Jurči, *Met. Sci. Heat Treat.* 63, 430 (2021).
26. I. Campos-Silva, E.J. Hernández-Ramirez, A. Contreras-Hernández, J.L. Rosales-Lopez, E. Valdez-Zayas, I. Mejía-Caballero, and J. Martínez-Trinidad, *Surf. Coat. Technol.* 421, 127404 (2021).
27. S. Ipekayvaz and I. Aydin, *Trans. Indian Inst. Met.* 73, 2635 (2020).
28. M. Arslan, M. Karimzadehkhoei, G.K. Sireli, O.K. Coskun, M. Sert, and S. Timur, *J. Mater. Eng. Perform.* 31, 3274 (2022).
29. A. Günen, B. Kurt, N. Orhan, and E. Kanca, *Prot. Met. Phys. Chem. Surf.* 50, 104 (2014).
30. Y. Kayali, A. Büyüksağış, I. Güneş, and Y. Yalçın, *Prot. Met. Phys. Chem. Surf.* 49, 348 (2013).
31. I. Gunes and I. Yıldız, *Rev. Mater.* 21, 61 (2016).
32. G. Kartal, S. Timur, V. Sista, O.L. Eryilmaz, and A. Erdemir, *Surf. Coat. Technol.* 206, 2005 (2011).
33. M. Keddama and M. Kulka, *Met. Sci. Heat Treat.* 62, 326 (2020).
34. A. Meneses-Amador, D. Blancas-Pérez, R. Corpus-Mejía, G. A. Rodríguez-Castro, J. Martínez-Trinidad, and L.F. Jiménez-Tinoco, *J. Mater. Eng. Perform.* 27, 2089 (2018).
35. O. Ozdemir, M.A. Omar, M. Usta, S. Zeytin, C. Bindal, and A.H. Ucisik, *Vacuum* 83, 175 (2008).
36. M. Çetin, A. Günen, M. Kalkandelen, and M.S. Karakaş, *Vacuum* 187, 110145 (2021).
37. S. Huang, D. Sun, W. Wang, and H. Xu, *Ceram. Int.* 41, 12202 (2015).
38. S.L. Liu and X.P. Zheng, *J. Alloys Compd.* 480, 254 (2009).
39. M. Ju Chao, W. Li Wang, E. Jun Liang, and D. Ouyang, *Surf. Coat. Technol.* 202, 1918 (2008).
40. A.K. Litoria, M.D. Joshi, V. Antunes, D. Singh, C.A. Figueroa, F. Alvarez, and S.S. Hosmani, *Philos. Mag.* 101, 777 (2021).
41. L. Lind, P. Peetsalu, and F. Sergejev, *Medziagotyra* 21, 343 (2015).
42. A. Günen, N. Makuch, Y. Altınay, C. Çarboğa, S. Dal, and Y. Karaca, *Ceram. Int.* 48, 36410 (2022).
43. C. Zhang, L. Liu, K.C. Chan, Q. Chen, and C.Y. Tang, *Intermetallics* 29, 80 (2012).
44. G.Y. Koga, R. Schulz, S. Savoie, A.R.C. Nascimento, Y. Drolet, C. Bolfarini, C.S. Kiminami, and W.J. Botta, *Surf. Coat. Technol.* 309, 938 (2017).
45. Q. Wang, Z.H. Chen, and Z.X. Ding, *Tribol. Int.* 42, 1046 (2009).
46. N. Ma, L. Guo, Z. Cheng, H. Wu, F. Ye, and K. Zhang, *Appl. Surf. Sci.* 320, 364 (2014).
47. A.C. Karaoglanlı, M. Oge, K.M. Doleker, and M. Hotamis, *Surf. Coat. Technol.* 318, 299 (2017).
48. J. Li, Y. Zhang, J. Huang, and C. Ding, *J. Therm. Spray Technol.* 7, 242 (1998).
49. T. Sahaoui, N.E. Fenineche, G. Montavon, and C. Coddet, *Mater. Des.* 24, 309 (2003).
50. M. Naeem, J.C. Díaz-Guillén, A. Khalid, I. Guzmán-Flores, R. Muñoz-Arroyo, J. Iqbal, and R.R.M. Sousa, *Tribol. Int.* 175, 3 (2022).
51. A. Erdogan, K.M. Döleker, and S. Zeytin, *Surf. Coat. Technol.* 399, 126179 (2020).
52. A. Erdoğan, *Proc. Inst. Mech. Eng. Part C J. Mech. Eng. Sci.* 236, 6873 (2022).
53. A. Günen, K.M. Döleker, M.E. Korkmaz, M.S. Gök, and A. Erdogan, *Surf. Coat. Technol.* 409, 126906 (2021).
54. T. Das, A. Erdogan, B. Kursuncu, E. Maleki, and O. Unal, *Surf. Coat. Technol.* 403, 126383 (2020).
55. K.M. Döleker, A. Erdogan, T. Yener, A.C. Karaoglanlı, O. Uzun, M.S. Gök, and S. Zeytin, *Surf. Coat. Technol.* 412, 127069 (2021).

Publisher's Note Springer Nature remains neutral with regard to jurisdictional claims in published maps and institutional affiliations.

Springer Nature or its licensor (e.g. a society or other partner) holds exclusive rights to this article under a publishing agreement with the author(s) or other rightsholder(s); author self-archiving of the accepted manuscript version of this article is solely governed by the terms of such publishing agreement and applicable law.